JOURNAL OF CATALYSIS 146, 268–276 (1994)

Influence of the *A*-Site Cation in $ACoO_3$ (*A* = La, Pr, Nd, and Gd) Perovskite-Type Oxides on Catalytic Activity for Methane Combustion

A. Baiker,*,[1] P. E. Marti,† P. Keusch,‡ E. Fritsch,§ and A. Reller§

*Department of Chemical Engineering and Industrial Chemistry, Swiss Federal Institute of Technology, ETH-Zentrum, CH-8092 Zürich, Switzerland; †Department of Combustion Technology, Paul Scherrer Institut, CH-5232 Villigen PSI, Switzerland; ‡Inorganic Chemistry Institute, University of Zürich, Winterthurerstrasse 190, CH-8057 Zürich, Switzerland; and §Inorganic and Applied Chemistry Institute, University of Hamburg, Martin-Luther-King-Platz-6, 2000 Hamburg 13, Germany

Received March 17, 1993; revised August 18, 1993

The effect of rare-earth ions (La, Pr, Nd, and Gd) in $ACoO_3$ perovskites on the thermal behavior and on the catalytic activity for methane oxidation has been studied. The thermal reduction, as investigated by oxygen desorption analysis, revealed for all perovskites one evolution step occurring above 1100 K. Transmission electron micrographs at the beginning of the desorption step revealed the presence of superstructures, which are attributed to the formation of oxygen-deficient domains ($ACoO_{2.5} \leq ACoO_{3-x} \leq ACoO_3$) adopting perovskite-related brownmillerite-type structures. A model for the sequence of the structural changes of the perovskites during the reduction is proposed. The amount of oxygen which evolved above 1100 K increased with decreasing size of the lanthanide ion. Comparative catalytic studies were carried out in a fixed-bed microreactor at atmospheric pressure in the temperature range 600–1200 K. The activities at 830 K, expressed as reaction rates referred to the BET surface area, increased in the order $PrCoO_3 \ll LaCoO_3 < NdCoO_3 < GdCoO_3$. However, no significant influence of the *A*-site cations on the catalytic activity was found, with exception of praseodymium. $PrCoO_3$ showed a 30 times lower activity than the other samples. The catalytic activity of $ACoO_3$ perovskites can be markedly affected by the presence of Co_3O_4 impurity in the perovskites. © 1994 Academic Press, Inc.

INTRODUCTION

The potential of perovskite-type oxides (general formula ABO_3) in catalysis was first reported by Parravano (1) in 1952 for CO oxidation. Since this early work numerous publications relevant to the application of these oxides in catalysis appeared. The perovskites containing a lanthanide in position *A* and a transition metal in position *B* have been found to be good catalysts for several reactions (2), such as oxidation of CO, hydrocarbons, and oxygenated compounds, reduction of NO_x, and hydrogenation of hydrocarbons, CO and CO_2, etc. Analogous studies have been carried out using perovskite-related structural frameworks, i.e., $La_{2-x}Sr_xNiO_{4-y}$ (3, 4) adopting the structure of the first member of the Ruddlesden–Popper phase series (5). Especially interesting is the application of perovskites in catalytic combustion devices with high heat throughput, such as gas turbines or industrial burners (6, 7). The relatively high oxidation activity of transition-metal oxides combined with the thermal stability of rare-earth oxides provide the perovskites the essential properties for these high-temperature applications. Arai *et al.* (8) investigated the catalytic combustion of methane over several $LaBO_3$ and $La_{1-x}Sr_xBO_3$ perovskites. Particularly the partly Sr-substituted $LaMnO_3$, $LaCoO_3$, and $LaFeO_3$ showed high oxidation activities comparable with the activity of Pt/Al_2O_3. High catalytic activities for methane combustion over perovskites were also reported by McCarty and Wise (9). An interesting characteristic of rare-earth perovskites is the possibility of varying the dimensions of the unit cell by varying the *A* ion, and thereby the covalence of the *B*–O bond in the ABO_3 structure. A thorough study of the role of the *A*- and *B*-site ions on the catalytic properties of ABO_3 perovskites for the oxidation of propane and methanol has been reported by Nitadori *et al.* (10). They concluded that the influence of the rare-earth ions in the *A*-site on the oxidation properties of these compounds were secondary, as long as they were trivalent. Zhang *et al.* (11) studied the oxygen sorption and catalytic properties for methane and *n*-butane combustion of $La_{1-x}Sr_xCo_{1-y}Fe_yO_3$. While the catalytic activity for *n*-butane oxidation was affected by transition-metal substitution as well as by rare-earth substitution, the catalytic activity for methane oxidation was only affected by rare-earth ion substitution.

In the present work we have studied comparatively the effects of the rare-earth ions in $ACoO_3$ perovskite-type

[1] To whom correspondence should be addressed.

0021-9517/94 $6.00

oxides on the thermal behavior and on the catalytic activity for the methane oxidation. X-ray diffraction, thermogravimetry, transmission electron microscopy, gas adsorption, and oxygen evolution measurements have been used to pursue this aim.

EXPERIMENTAL

Catalysts

The catalysts were prepared by calcination of water-insoluble hydroxides mixtures, using fresh calcined simple oxides as start materials, La_2O_3, Pr_6O_{11}, Nd_2O_3, Gd_2O_3, and Co_3O_4, obtained from Fluka (puriss). Rare-earth oxides (0.0165 mol, referred to the cation) were dissolved in a solution of nitric acid (5 *M*, 12 ml). The dissolution of Co_3O_4 (0.0165 mol, referred to the cation) in concentrated nitric acid was facilitated by dropwise addition of H_2O_2. The volume of the solution was completed to 100 ml with deionized water and added dropwise together with an aqueous solution of tetramethyl ammonium hydroxide (2.8 *M*, Fluka, pract.) to 100 ml of deionized water at 303 K and at a constant pH of 9.0, with vigorous stirring. The precipitated hydroxides were separated from the liquid by centrifugation and washed two times with deionized water. Barnard *et al.* (12) have reported for $LaCoO_3$ that samples which were washed with acetone before dehydration had higher surface areas than samples which were directly dehydrated by air-drying. Based on this experience the precipitate was washed with acetone before drying at 400 K in air and subsequently calcined in air at 1070 K for 10 h and finally at 1170 K for 12 h. The catalysts were pressed, crushed, and sieved. The size fraction between 100 and 300 μm was used for catalytic tests and nitrogen physisorption measurements.

Samples were also prepared starting from commercial hydrous metal nitrates (Fluka, puriss p.a.) employing a technique similar to that described by Vidyasagar *et al.* (13); however, the use of chlorine as oxidant was omitted. This preparation led to perovskites which were contaminated with Co_3O_4.

Physicochemical Characterization

The phase identification of the catalysts was carried out by powder X-ray diffractometry using a Siemens D5000 diffractometer. Conditions were: CuK_α radiation, 20 mA, 25 kV, Ni-filter, step scan size = 0.0009°. The patterns obtained were compared with JCPDS data files.

Physisorption measurements were performed with a Micromeritics Asap 2000 instrument. The BET surface areas were determined by nitrogen adsorption at 77 K in the relative pressure range $0.05 \leq p/p^0 \leq 0.20$ assuming a cross-sectional area of 0.162 nm^2 for the nitrogen molecule. Prior to the adsorption measurements the samples were outgassed in vacuum at 423 K for 4 h.

Thermoanalytical investigations were carried out using a Mettler thermoanalyzer (TA 2000 C). Approximately 15 mg of the sample were placed in a platinum sample pan and heated at 10 K/min from room temperature to 1270 K. High purity gases (Ar, 99.998; H_2, 99.999) passed through the sample chamber (25 ml/min) at atmospheric pressure. As a reference, α-Al_2O_3 was used.

Temperature-programmed desorption (TPD) of oxygen was measured in a flow system. Each sample (0.100 g) was placed in a fused-quartz microreactor and pretreated in a stream (300 ml/min STP) of 4% O_2 and 96% He at 1120 K for 1 h. The sample was then cooled to room temperature in the same atmosphere and subsequently heated in a He stream (300 ml/min STP) at a constant heating rate of 10 K/min. The evolving oxygen was monitored with an on-line quadrupole mass spectrometer (Balzers GAM 445).

Transmission electron microscopy was carried out using a JEOL 200CX equipped with a top entry stage. The samples were gently crushed in an agate mortar, dispersed in hexane, and subsequently disposed on a copper grid coated with an amorphous holey carbon film.

Catalytic Tests

Kinetic studies were performed in a continuous fixed-bed microreactor operated at atmospheric pressure. The reactor was a 6-mm-o.d. and 4-mm-i.d. fused-quartz tube, placed vertically in an electric furnace. The catalyst temperature was monitored by a chromel–alumel thermocouple separated from the catalyst bed by a 0.2-mm-thick quartz wall. To preheat the reactant gas and to obtain a uniform velocity profile, quartz-wool was placed before and after the catalyst bed. The reactant feed rate was controlled by mass flow controllers (Brooks 5850E). Both inlet and outlet gas compositions were quantitatively analyzed using an on-line quadrupole mass spectrometer (Balzers GAM 445). Comparative activity tests were carried out under the following conditions: reactant feed, 1% CH_4 (99.995%), 4% O_2 (99.999%) and 95% He (99.998%); catalyst load, 0.100 g mixed with 0.100 g SiO_2 powder to reduce the heat release per unit volume; the gas flow rate was adjusted to obtain a gas hourly space velocity (GHSV) of 135,000 h^{-1}. The temperature was increased stepwise from 570 to 1150 K. Reported activities are steady-state values measured after steady-state conversion has been attained. After completion of the whole test series the measurement at 870 K was repeated to confirm the stationarity of the catalyst activity during the kinetic test. The methane conversion to CO_2 was calculated from a carbon balance: $P_{CO_2}/(P_{CH_4} + P_{CO_2} + P_{CO}) \cdot 100$, where P_{CH_4}, P_{CO_2}, and P_{CO} are the partial pressures of CH_4, CO_2, and CO, respectively.

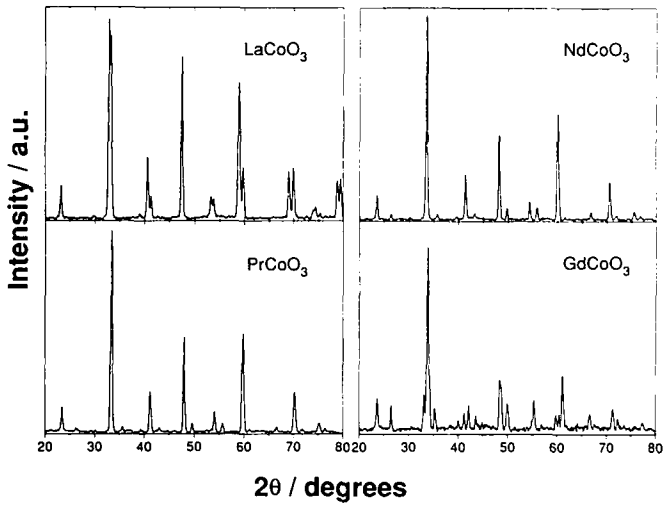

FIG. 1. XRD powder patterns (CuK_α) of the investigated perovskites.

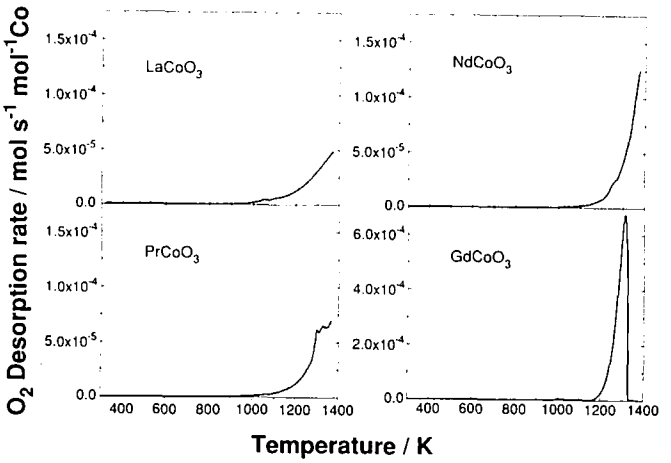

FIG. 2. Temperature-programmed oxygen evolution from $LaCoO_3$, $PrCoO_3$, $NdCoO_3$, and $GdCoO_3$. Sample weight, 0.1 g; carrier gas, He (300 ml/min); heating rate, 10 K/min.

The criterion of Koros and Nowak (14) has been applied to determine whether the conversion was limited by transport phenomena or not. Powders of $NdCoO_3$ (0.5 g), which was the catalyst with the highest overall activity, and SiO_2 (0.5 g) were well mixed, pressed, crushed, and sieved, and the size fraction from 100 to 300 μm was used for the diagnostic test. Up to 780 K the conversion of methane over $NdCoO_3$ (20%) was two times higher than the conversion over the 1 : 1 $NdCoO_3$: SiO_2 mixture, indicating that below this temperature (conversion <20%) mass-transport limitations were not important.

RESULTS

Bulk Structure and Physisorption Measurements

The formation of the perovskite phase in all catalysts was confirmed by XRD (Fig. 1), showing sharp, well-defined perovskite peaks. As evidenced by the XRD patterns, $LaCoO_3$ has a rhombohedral, $PrCoO_3$ and $NdCoO_3$ a cubic, and $GdCoO_3$ an orthorhombic structure.

BET surface areas of $LaCoO_3$, $PrCoO_3$, $NdCoO_3$, and $GdCoO_3$ were 3.5, 5.1, 1.6, and 2.1 m^2/g, respectively. Nitrogen sorption measurements showed for all samples type IV isotherms with very little hysteresis of type H1, according to the IUPAC classification (15), at high relative pressures (>0.95). This feature is typical for porous adsorbents consisting of agglomerates. The *t*-plots confirmed the absence of micropores.

TABLE 1

Results of the Reduction in Pure Hydrogen

Catalyst	T_{max}[a] (K)	Change in the nonstoichiometry[b] (as δ in $ACoO_{3-\delta}$)	Crystallographic phases[c]
$LaCoO_3$	633	0.72	Analogous to the parent perovskite
	823	0.81	$La(OH)_3$, Co
$PrCoO_3$	623	0.66	Not isolated
	653	0.64	PrO_2, Co, unknown phase
	813	0.71	PrO_2, Co
$NdCoO_3$	633	0.77	Analogous to the parent perovskite
	793	0.77	Nd_2O_3, Co
$GdCoO_3$	663	0.67	Analogous to the parent perovskite
	773	0.82	Gd_2O_3

[a] Temperature at which the reduction rate reached a maximum.
[b] Calculated from $\delta = [\Delta m - MG(ACoO_3)]/[m_0 - MG(O)]$, where Δm is the sample weight loss, m_0 is the initial sample weight, $MG(ACoO_3)$ is the molecular weight of the perovskite, and MG(O) = 16.
[c] According to the XRD patterns.

Thermal Behavior in Hydrogen

The thermal behavior under a pure hydrogen atmosphere was examined by thermogravimetry. Under the

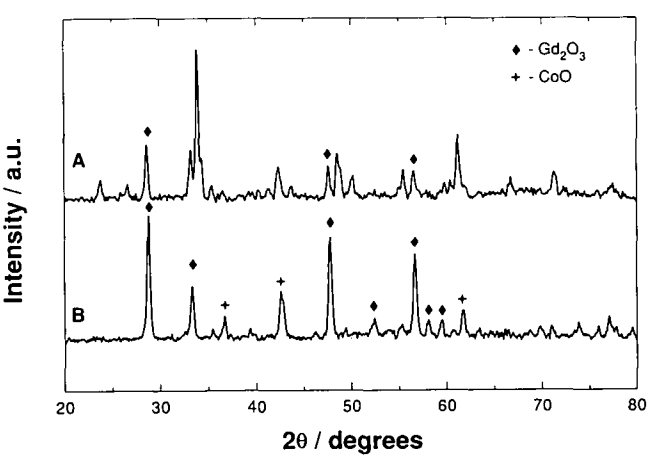

FIG. 3. XRD patterns of $GdCoO_3$ after TPD experiments: (A) Heated up to 1300 K and (B) heated up to 1370 K, i.e., until completion of the peak.

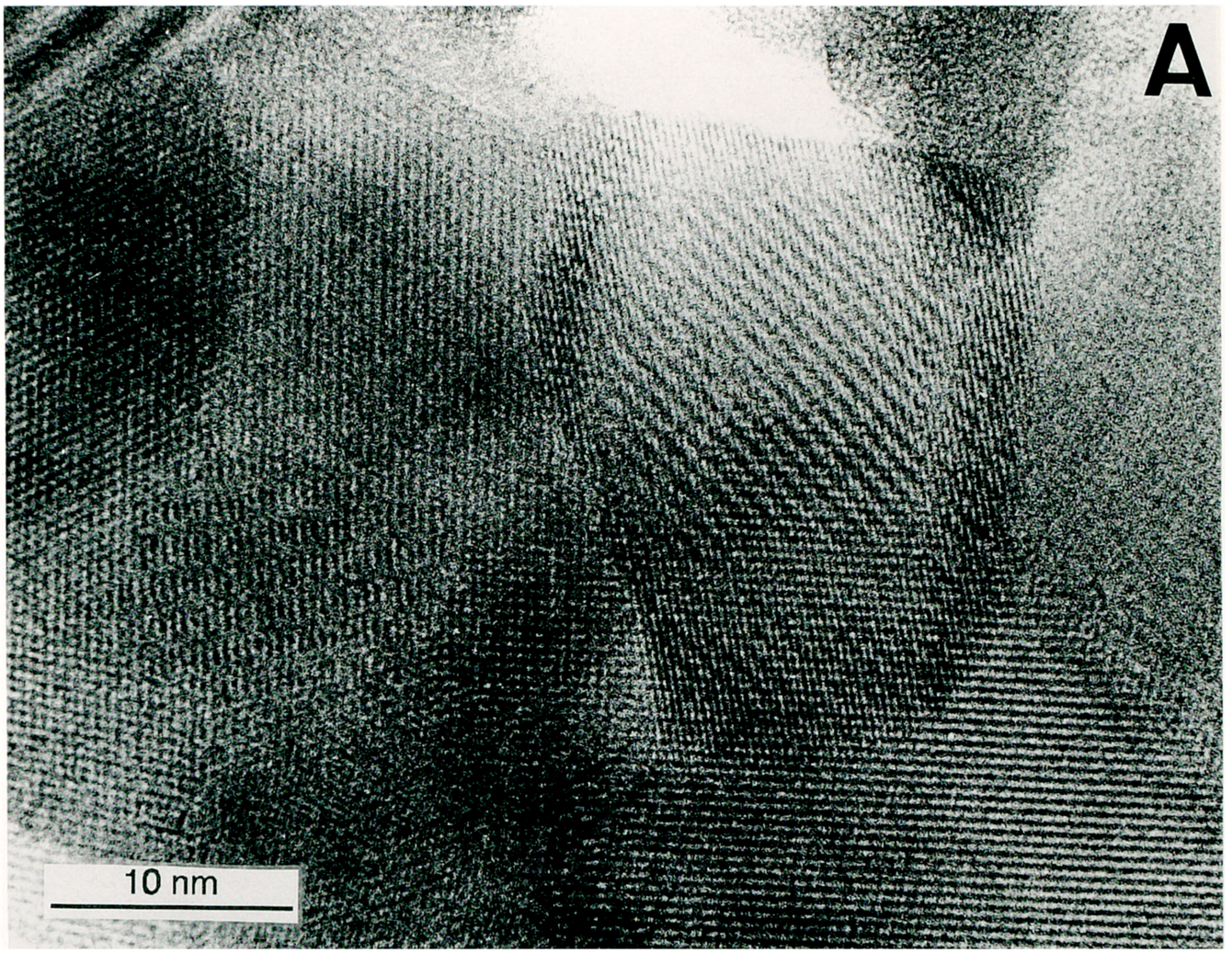

FIG. 4. Transmission electron micrographs of microdomains of $GdCoO_{3-x}$ (A) and $NdCoO_{3-x}$ (B). The contrast patterns show, that the size of coherent crystalline domains varies between several hundred and few thousand Å in diameter. They also give evidence for the presence of ordered oxygen vacancies causing superstructures (particularly well visible in (B)).

experimental conditions used (heating rate 10 K/min) the reduction occurred in two steps for $LaCoO_3$, $NdCoO_3$, and $GdCoO_3$, and in three steps for $PrCoO_3$ (see also Ref. (16)). The temperature at which the maximum of the reduction rate is achieved (T_{max}), the weight loss, the corresponding change in the stoichiometry and the phases detected (XRD) during the reduction are listed in Table 1. The weight loss in the first stage can be associated to the complete reduction of Co^{+3} to Co^{+2}. This leads to the formation of the perovskite-related brownmillerite-type intermediate $ACoO_{2.5}$. Its structure is made up of corner-sharing CoO_6 octahedra and CoO_4 tetrahedra (17). The formation of this anion-deficient perovskite-related phases demands the diffusion of bulk oxygen ions to the surface. This diffusion processes are rather slow. Consequently surface-near domains can undergo full reduction of the Co^{+3} and Co^{+2} to Co^0, while there is still bulk material present with stoichiometries in the range of $ACoO_3 \leq ACoO_{3-x} \leq ACoO_{2.5}$, as detected by X-ray diffraction. Interestingly, with $PrCoO_3$, PrO_2 was produced and not Pr_2O_3 as expected. It has been suggested (18) that praseodymium could participate in the redox reaction and be oxidized from Pr^{+3} to Pr^{+4}, while Co^{+3} or Co^{+2} are reduced. $PrCoO_3$ is, compared with the isostructural compounds $LaCoO_3$, $NdCoO_3$, and $GdCoO_3$, readily reducible to the segregate oxides. This behavior can also be related with the role of praseodymium as redox-active species.

Upon exposure of the freshly reduced $LaCoO_3$ sample to air at room temperature $La(OH)_3$ formed very quickly,

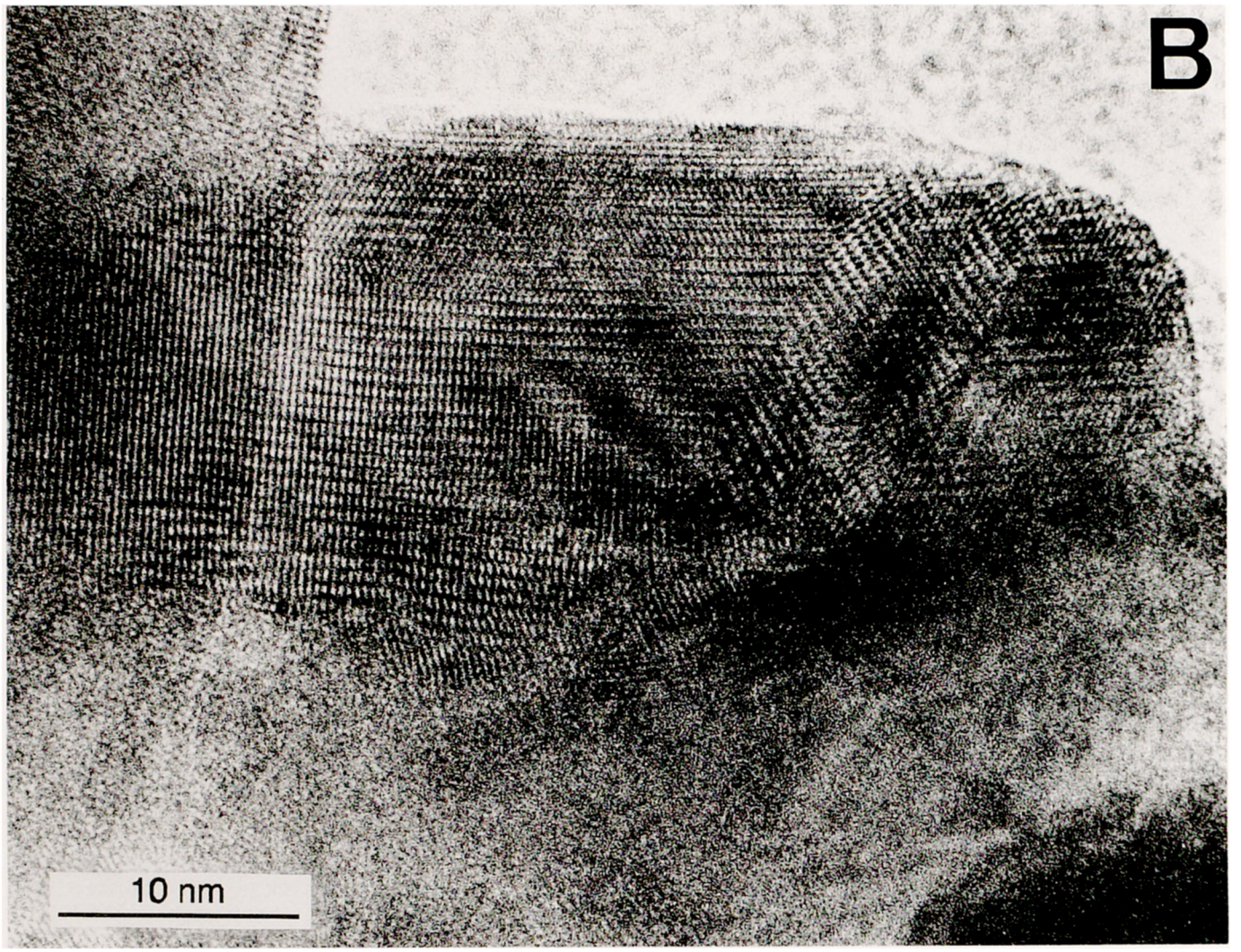

FIG. 4—*Continued*

accompanied with a temperature rise. The same behavior has been reported by Crespin and Hall (19).

Temperature-Programmed Desorption of Oxygen

The oxygen evolution profiles of the four catalysts are depicted in Fig. 2. The rate of oxygen desorption per mol of cobalt present in the sample is plotted as a function of the catalyst temperature. Note the different ordinate scale for $GdCoO_3$. All samples showed one desorption peak beginning around 1100 K, which was only for $GdCoO_3$ completed below 1370 K.

Figure 3A shows the XRD pattern of $GdCoO_3$ after heating it to 1300 K in He. Reflections corresponding to the perovskite phase and the simple oxides can be observed, indicating that segregation takes place. After completion of the desorption peak at 1370 K, only Gd_2O_3 and CoO were detected (Fig. 3B).

Transmission electron micrographs of $GdCoO_{3-x}$ (Fig. 4A) and $NdCoO_{3-x}$ (Fig. 4B), taken at the beginning of the oxygen evolution, give evidence that on one side the size of coherent crystalline microdomains varies between few hundred and few thousand Å in diameter, on the other side superstructures are present. These superstructures, clearly visible in the case of $NdCoO_{3-x}$, are a consequence of the formation of oxygen-deficient domains adopting the mentioned perovskite-related brownmillerite structure.

The amount of evolved oxygen was calculated by integrating the oxygen desorption rate with time. The amount of oxygen that evolved from 800 to 1370 K increases with decreasing size of the lanthanide ion (Fig. 5). The relative

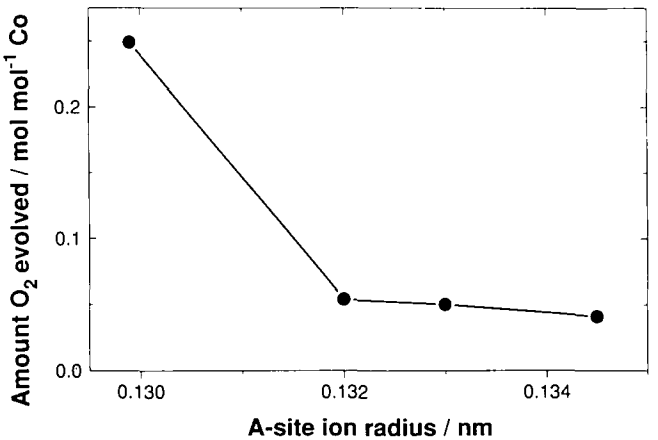

FIG. 5. Relation between amount of oxygen which evolved above 1100 K during the TPD measurements and the ionic radius of the lanthanide ions. The ionic radii were taken from (23).

effective ionic radii, with coordination number 12, of the trivalent rare-earth cations calculated from perovskites were taken from (20). This is in accordance with the increasing stability of the perovskite structure with increasing size of the lanthanide ion reported (21).

Catalytic Activity

Preliminary tests carried out with 0.100 g of SiO_2 under the same reaction conditions as used for the activity tests showed negligible methane conversion below 1000 K. At 1100 K predominantly H_2O (710 ppm), CO (260 ppm), and CO_2 (110 ppm) were formed. The temperature dependencies of the methane oxidation over the four catalysts are shown in Fig. 6. The catalytic activities were compared at a constant GHSV of 135,000 h^{-1}. $NdCoO_3$ showed the highest overall activity, what can be attributed to the

TABLE 2

Kinetic Results of the Investigated Catalysts

Catalyst	E_a[a] (kJ/mol)	$T_{50\%}$[b] (K)	Reaction rate[c] (mol/s m^2 × 10^{-6})
$LaCoO_3$	104 ± 1	982	0.36
$PrCoO_3$	110 ± 10	1176	0.014
$NdCoO_3$	103 ± 2	931	0.48
$GdCoO_3$	99 ± 2	1006	0.50

[a] Apparent activation energy with 95% confidence limits.
[b] Temperature at which 50% methane conversion was attained.
[c] Calculated at 830 K.

larger surface area of this catalyst compared to the others. Note the low overall activity of $PrCoO_3$. Reaction rates, temperatures at which 50% of methane oxidation is attained ($T_{50\%}$), and apparent activation energies (Ea) are summarized in Table 2, and a comparison of the Arrhenius plots is shown in Fig. 7. The apparent activation energies were calculated at conversions below 10%. They vary between 99 and 110 kJ/mol. The reaction rates referred to the BET surface area and measured at 830 K showed, with exception of $PrCoO_3$, only a slight dependence on the *A*-site ion size, i.e., the smaller the *A*-site ion the higher the catalytic activity. The low specific activity of $PrCoO_3$ could be related to the redox properties of the Pr^{+4}/Pr^{+3} system, which influence the valence state of the cobalt ion under reaction conditions. However, further work is necessary to clarify this point.

Effect of Co_3O_4 Impurity on the Thermal Behavior and on the Catalytic Activity

As already mentioned in the Experimental section, perovskite samples have also been prepared starting from

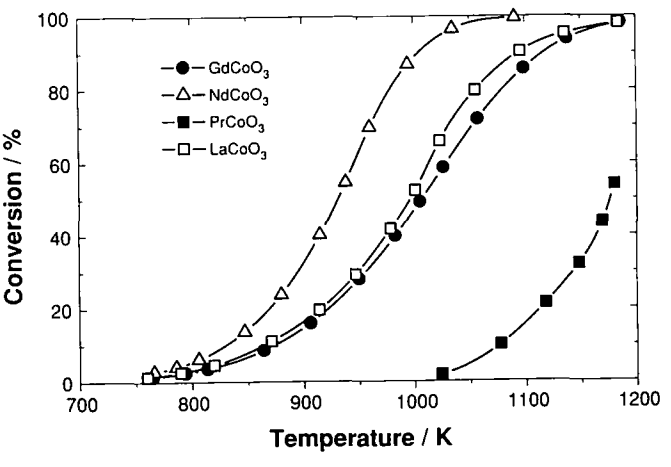

FIG. 6. Comparison of the overall activities of the four catalysts. Reactant gas composition, 1% CH_4, 4% O_2, He (balance); sample weight, 0.1 g; GHSV, 135,000 h^{-1}.

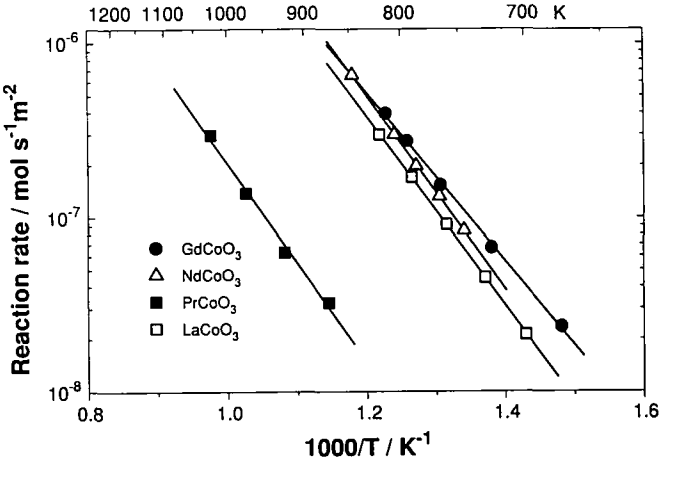

FIG. 7. Arrhenius plots of the methane combustion rates measured for the four catalysts. Reactant gas composition, 1% CH_4, 4% O_2, He (balance); sample weight, 0.1 g; GHSV, 135,000 h^{-1}.

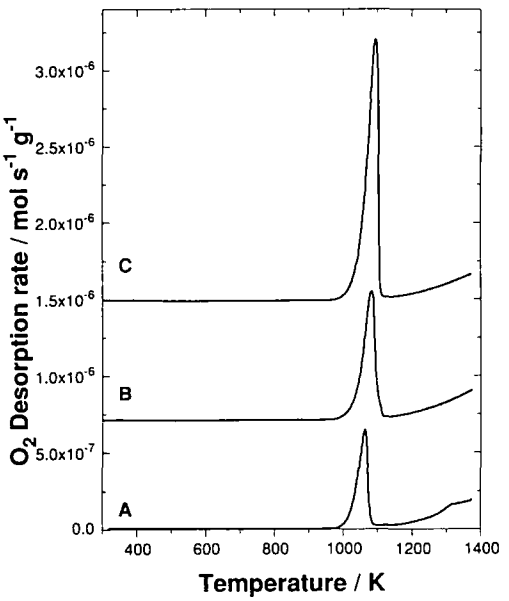

FIG. 8. Temperature-programmed oxygen evolution from $LaCoO_3$: (A) sample prepared from commercial hydrous metal nitrates; (B) sample prepared from metal oxides, with 10 wt% Co_3O_4; (C) sample prepared from oxides, with 20 wt% Co_3O_4. Sample weight, 0.1 g; carrier gas, He (300 ml/min); heating rate, 10 K/min.

commercial hydrous metal nitrates. Using this method, absolutely pure perovskites could not be prepared with $PrCoO_3$ and $GdCoO_3$, where XRD patterns revealed the presence of small amounts of Pr_6O_{11} and Gd_2O_3, respectively. TPD measurements carried out with these samples revealed for all perovskites two discernable reduction steps occurring in the range 100–1100 K and above 1100 K, respectively. The corresponding TPD profile for $LaCoO_3$ is depicted in Fig. 8A. The low-temperature (1050 K) oxygen desorption from $LaCoO_3$ has been associated (22, 23) with the evolution of lattice oxygen which accompanied the partial reduction of some Co^{+3} to Co^{+2}, without affecting the unit cell of the perovskite structure. The formation of Co_3O_4 impurity in $LaCoO_3$, which decomposes around 1070 K, has been proposed earlier (9). The present studies provide further evidence that the desorption at this low temperature has to be attributed to the presence of Co_3O_4 impurity. To determine whether the oxygen which evolves at 1050 K originates from the perovskite lattice or from Co_3O_4, $LaCoO_3$ samples containing 10 and 20 wt% Co_3O_4 in excess were prepared, starting from the oxides. Their TPD profiles are shown in Figs. 8B and 8C, respectively. The amount of oxygen which evolved was integrated, and the results summarized in Table 3. The amount of oxygen which evolved from 800 to 1110 K correlates linearly with the content of Co_3O_4 in the samples, indicating that the low temperature oxygen evolution from $LaCoO_3$ (prepared from nitrates) can be attributed to the presence of Co_3O_4 impurity (around wt%).

TABLE 3

Characteristic Data of Oxygen Desorption Measurements

Catalyst	T_{max}[a] (K)	Amount oxygen evolved 800–1110 K	Amount oxygen evolved 1110–1370 (μmol/g)
$LaCoO_3$[c]	—	—	160
$LaCoO_3$ + 10 wt% Co_3O_4[c]	1078	230	140
$LaCoO_3$ + 20 wt% Co_3O_4[c]	1095	430	130
$LaCoO_3$[d]	1062	150	140

[a] Temperature at which the oxygen desorption rate reached maximum.

[b] Oxygen which evolved from 0.1 g sample into 300 ml/min He at heating rate of 10 K/min following treatment at 1120 K in 4% O_2 a 96% He for 1 h.

[c] Prepared from the oxides.

[d] Prepared from the nitrates.

Figure 9 compares the reaction rates referred to th BET surface area of $LaCoO_3$ prepared from the consti uent oxides, $LaCoO_3$ prepared from the metal nitrate containing 7 wt% Co_3O_4, as evidenced by TPD, and mechanical mixture of La_2O_3 and Co_3O_4 containing th constituents in a molar ratio Co/La of 1 : 1. Before us the oxides of the mechanical mixture were calcined 870 K for 6 h. The activity of this mixture has been r ferred to the surface area of Co_3O_4 (10.5 $m^2\ g^{-1}$). No that the activity of the contaminated perovskite (fro nitrate precursors) lies in the same range as the activi

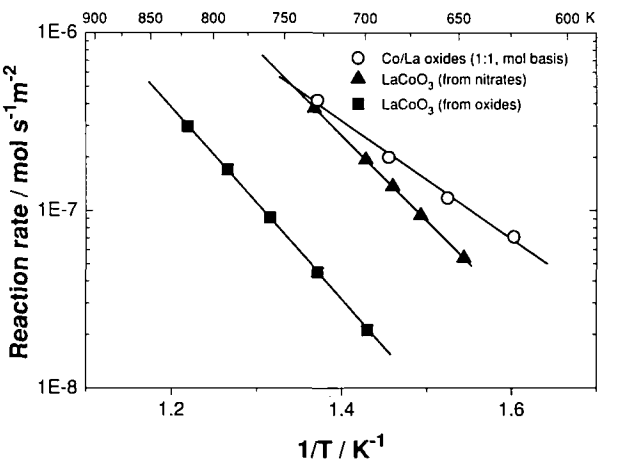

FIG. 9. Arrhenius plots of the methane combustion rate measur for $LaCoO_3$ prepared from metal nitrates and from metal oxides, a for a mechanical mixture of Co_3O_4/La_2O_3 with a molar ratio Co/La 1. Reactant gas composition, 1% CH_4, 4% O_2, He (balance); sam weight, 0.1 g; GHSV, 135,000 h^{-1}.

of the Co_3O_4/La_2O_3 sample, whereas the activity of the pure perovskite is about an order of magnitude lower.

DISCUSSION

The lanthanides are chemically very similar and many of their properties can be explained on the base of the different ionic radii and charge densities of their constituents. The ionic radius of the trivalent lanthanides decrease with increasing atomic number in a period of the periodic table. An increasing distortion of the ideal cubic perovskite structure with decreasing ionic radius was reported by Marezio *et al.* (24) for $AFeO_3$ and by Demazeau *et al.* (25) for $ANiO_3$ perovskites. Arakawa *et al.* (26) found by the reduction of $ACoO_3$ perovskites in a hydrogen atmosphere an increasing amount of oxygen deficiency in the order La < Nd < Sm = Eu. The oxygen evolution experiments of the present study show that the nature of the lanthanide ions strongly influences the reducibility of the Co^{+3} ions. The TPD profiles (Fig. 2) indicate that the oxygen evolution occurs in one step, starting from 1100 K. Heating the samples at temperatures above 1100 K produces a phase segregation, with formation of the simple oxides. The high-temperature desorption (Fig. 5) shows a clear dependence on the lanthanide ion: the smaller the rare-earth cation the greater the total amount of oxygen evolved from 800 to 1370 K, i.e., the amount of oxygen which evolved correlates inversely with the energy of the metal-oxygen bond. For $GdCoO_3$ the segregation is completed below 1370 K:

$$GdCoO_3 \rightarrow \tfrac{1}{2}Gd_2O_3 + CoO.$$

The mechanistic course of the thermal reduction and the reduction in hydrogen can be explained by the following processes (Fig. 10): Starting from the perovskite structure the reduction leads to the formation of firstly lacunary oxygen vacancies (see also (27)). As soon as a given oxygen loss occurs, oxygen vacancies tend to order and superstructures of the parent perovskite framework are observed. These superstructures adopt brownmillerite-type frameworks made up of layers of corner-sharing CoO_4 tetrahedra and CoO_6 octahedra. In the stoichiometric range between $ACoO_3 \geq ACoO_{3-x} \geq ACoO_{2.5}$ the formation of various structures with different ratios of tetrahedral to octahedral sheets allow the reversible release and uptake of oxygen, i.e., probably the crucial process for the observed catalytic activity. It is to expect, that the substitution of Co by, e.g., Mn, Ni, or Fe not only influences the mechanism of formation of non-stoichiometric structures (28) but concomitantly the catalytic activity.

Nitadori *et al.* (10) found for the oxidation of propane and methanol over $ACoO_3$ perovskites that the role of the rare-earth ions on the catalytic activity was less influential than the one of the transition metal ions. Le Coustumer (29) reported comparable activity values for methane combustion over various cobaltites with spinelle and perovskite structure. However, a correlation between the catalytic activity and the surface oxygen binding energy has been found by Futai *et al.* (30) for the oxidation of CO over $ACoO_3$ perovskites.

In our study, the changes in the physical properties of the lanthanides had not a significant effect upon the catalytic activity of the perovskites for methane oxidation. $LaCoO_3$, $NdCoO_3$, and $GdCoO_3$ showed a slight increase of the reaction rate with decreasing lanthanide

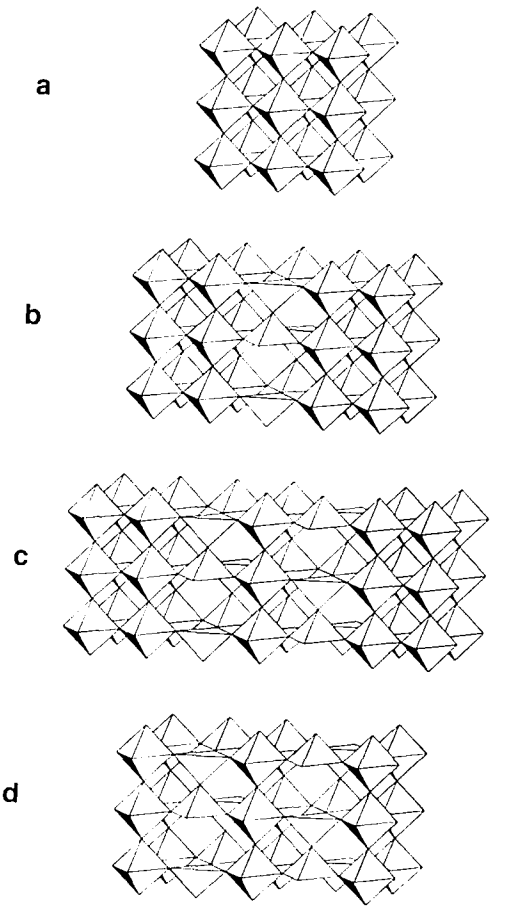

FIG. 10. Schematic representation of the structural changes concomiting the transformation of the parent perovskite structure into the brownmillerite structure. (a) Framework of the corner-sharing CoO_6 octahedra. Partial reduction, i.e., insertion of oxygen vacancies leads to the formation of corner-sharing layers of CoO_6 octahedra and CoO_4 tetrahedra. Whereas the thickness of the octahedral layers may vary, only isolated tetrahedral layers can be stabilized between octahedral ones. (b) An intermediate ABO_{3-x} structure with an unordered sequence. (c) A structure with an ordered sequence of 2 octahedra/1 tetrahedron leading to an ordered superstructure and a defined stoichiometry of $ABO_{2.75}$. Finally, the $ABO_{2.5}$ brownmillerite structure shown in (d) is made up even amounts of alternating octahedral and tetrahedral layers.

ion size. $PrCoO_3$ showed a 10 times lower activity than the other cobaltites. However, praseodymium was the only lanthanide investigated here which is bivalent. Due to the possible coexistence of the two oxidation states of praseodymium (3 and 4) in $PrCoO_3$, it seems feasible that the required charge compensation is achieved by the formation of Co^{+2}: $Pr^{+3}_{1-x}Pr^{+4}_{x}CO^{+3}_{1-x}Co^{+2}_{x}O_3$, resulting in a collapse of the activity. However, this argumentation needs further experimental proof.

The presence of Co_3O_4 impurity in the $ACoO_3$ samples influences strongly their catalytic activity. As has been shown for $LaCoO_3$, a contamination of 7 wt% with X-ray amorphous Co_3O_4 can enhance the activity of the perovskite by a factor of 10, making it comparable with the activity of bulk Co_3O_4. Preparation of mixed oxides starting from the hydrous metal nitrates can be accompanied with the formation of one of the simple oxides in excess. This is due mainly to the hygroscopic properties of several nitrates salts, making the determination of the exact amount of metal difficult.

CONCLUSIONS

The nature of lanthanide ions strongly influences the reducibility of the Co^{+3} ions in $ACoO_3$ perovskites, as revealed by oxygen evolution experiments. The smaller the rare-earth cation the greater the total amount of oxygen which evolves above 1100 K, i.e., the smaller the lanthanide cation the less stable the perovskite structure. This corroborates earlier work (21), where an increase of the reducibility in hydrogen of $ACoO_3$ oxides with decreasing size of the lanthanide ions has been found. The reduction process leads first to the formation of lacunary oxygen vacancies. As soon as a given oxygen loss occurs the vacancies tend to order and superstructures of the perovskite framework adopting brownmillerite-type structures are formed. The *A*-site cations have no much influence on the catalytic activity of the perovskites, with exception of praseodymium. $PrCoO_3$ has approximately 30 times lower activity than the others samples. The catalytic activity of these cobaltites can be significantly influenced by the presence of Co_3O_4 impurity.

ACKNOWLEDGMENT

We thank the Bundsamt für Energiewirtschaft (BEW) for financial support of this work.

REFERENCES

1. Parravano, G., *J. Chem. Phys.* **20,** 342 (1952).
2. Tejuca, L. G., Fierro, J. L., and Tascón, J. M. D., *Adv. Catal.* **36,** 237 (1989).
3. Ladavos, A. K., and Pomonis, P. J., *J. Chem. Soc. Faraday Trans.* **87,** 3291 (1991).
4. Ladavos, A. K., and Pomonis, P. J., *J. Chem. Soc. Faraday Trans.* **88,** 2557 (1992).
5. Ruddlesden, S. N., and Popper, P., *Acta Crystallogr.* **11,** 54 (1958).
6. Arai, H., and Machida, M., *Catal. Today* **10,** 81 (1991).
7. Kesselring, J. P., *in* "Advanced Combustion Methods" (F. J. Weinberg, Ed.). Academic Press, London, 1986.
8. Arai, H., Yamada, T., Eguchi, K., and Seiyama, T., *Appl. Catal.* **26,** 265 (1986).
9. McCarty, J. G., and Wise, H., *Catal. Today* **8,** 231 (1990).
10. Nitadori, T., Ichiki, T., and Misono, M., *Bull. Chem. Soc. Jpn.* **61,** 621 (1988).
11. Zhang, H. M., Shimizu, Y., Teraoka, Y., Miura, N., and Yamazoe, N., *J. Catal.* **121,** 432 (1990).
12. Barnard, K. R., Foger, K., Turney, T. W., and Williams, R. D., *J. Catal.* **125,** 265 (1990).
13. Vidyasagar, K., Gopalakrishnan, J., and Rao, C. N. R., *J. Solid State Chem.* **58,** 29 (1985).
14. Koros, R. M., and Nowak, E. J., *Chem. Eng. Sci.* **22,** 470 (1967).
15. Sing, K. S. W., Everett, D. H., Haul, R. A. W., Moscou, L., Pierotti, Rouquérol, J., Siemieniewska, T., *Pure Appl. Chem.* **57,** 603 (1985).
16. Vidyasagar, K., Reller, A., Gopalakrishnan, J., and Rao, C. N. R., *J. Chem. Soc. Chem. Commun.*, 7 (1985).
17. Beggren, J., *Acta Chem. Scand.* **25,** 3616 (1971).
18. Doka, G., Diploma work, Inorganic Chemical Institute, University of Zürich, 1990.
19. Crespin, M., and Hall, K., *J. Catal.* **69,** 359 (1981).
20. Espinosa, G. P., *J. Chem. Phys.* **37,** 2344 (1962).
21. Arakawa, T., Ohara, N., and Shiokawa, J., *J. Mater. Sci.* **21,** 1824 (1986).
22. Yamazoe, N., Furukawa, S., Teraoka, Y., and Seiyama, T., *Chem. Lett.*, 893 (1984). Yamazoe, N., Furukawa, S., Teraoka, Y., and Seiyama, T., *Chem. Lett.*, 2019 (1982).
23. Seiyama, T., *in* "Properties and Applications of Perovskite-Type Oxides" (L. G. Tejuca and J. L. G. Fierro, Eds.). New York, 1993.
24. Marezio, M., Remika, J. P., and Dernier, P. D., *Acta Crystallogr. Sect. B* **26,** 2008 (1970).
25. Demazeau, G., Marbeuf, A., Pouchard, M., and Hagenmüller, P., *J. Solid State Chem.* **3,** 582 (1971).
26. Arakawa, T., Ohara, N., and Shiokawa, J., *Chem. Lett.*, 1467 (1984).
27. Komornicki, S., Grenier, J. C., Pouchard, M., and Hagenmüller, P., *Nouv. J. Chim.* **5,** 161 (1981).
28. Reller, A., and Williams, T. B., *Chem. Br.* **25,** 1227 (1989).
29. Le Coustumer, L. R., Thesis Nr. 604, Univ. of Science and Technology of Lille, France, 1983.
30. Futai, M., Yonghua, C., and Louhui, *React. Kinet. Catal. Lett.* **31,** 47 (1986).